AD-A126 115 THEORY OF GYROTRON AMPLIFIERS IN A DISK OR A HELIX LOADED WAVEGUIDE(U) NAVAL SURFACE WEAPONS CENTER SILVER SPRING MD J Y CHOE ET AL. DEC 82 NSWC/TR-82-526 1/1

UNCLASSIFIED SBI-AD-F500 143 F/G 9/2 NL

END

FILMED

DTIC

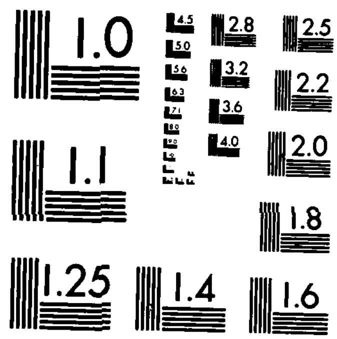
1.0
4.5
5.0
5.6
6.3
7.1
8.0
9.0
2.8
3.2
3.6
4.0
2.5
2.2
2.0
1.1
1.8
1.25
1.4
1.6

NSWC TR 82-526
PLASMA PHYSICS PUBLICATION NO. 82-12

THEORY OF GYROTRON AMPLIFIERS IN A DISK OR A HELIX LOADED WAVEGUIDE

BY JOON Y. CHOE,
HAN S. UHM

RESEARCH AND TECHNOLOGY DEPARTMENT

DECEMBER 1982

NAVAL SURFACE WEAPONS CENTER

Dahlgren, Virginia 22448 • Silver Spring, Maryland 20910

UNCLASSIFIED

SECURITY CLASSIFICATION OF THIS PAGE (When Data Entered)

REPORT DOCUMENTATION PAGE		READ INSTRUCTIONS BEFORE COMPLETING FORM
1. REPORT NUMBER NSWC TR 82-526	2. GOVT ACCESSION NO. AD-A126 115	3. RECIPIENT'S CATALOG NUMBER
4. TITLE (and Subtitle) THEORY OF GYROTRON AMPLIFIERS IN A DISK OR A HELIX LOADED WAVEGUIDE		5. TYPE OF REPORT & PERIOD COVERED 6. PERFORMING ORG. REPORT NUMBER
7. AUTHOR(s) Joon Y. Choe and Han S. Uhm		8. CONTRACT OR GRANT NUMBER(s)
9. PERFORMING ORGANIZATION NAME AND ADDRESS Naval Surface Weapons Center (Code R41) White Oak Silver Spring, MD 20910		10. PROGRAM ELEMENT, PROJECT, TASK AREA & WORK UNIT NUMBERS 61152N; ZR00001; ZR01109; R01AA400
11. CONTROLLING OFFICE NAME AND ADDRESS		12. REPORT DATE December 1982 13. NUMBER OF PAGES 46
14. MONITORING AGENCY NAME & ADDRESS(if different from Controlling Office)		15. SECURITY CLASS. (of this report) UNCLASSIFIED 15a. DECLASSIFICATION/DOWNGRADING SCHEDULE

16. DISTRIBUTION STATEMENT (of this Report)

Approved for public release; distribution unlimited.

17. DISTRIBUTION STATEMENT (of the abstract entered in Block 20, if different from Report)

18. SUPPLEMENTARY NOTES

19. KEY WORDS (Continue on reverse side if necessary and identify by block number)

Gyrotron Amplifiers
Disk Loaded Waveguide
Helix Loaded Waveguide

20. ABSTRACT (Continue on reverse side if necessary and identify by block number)

The gyrotron amplifiers in two slow wave structures, the disk and the helix loaded waveguides, are investigated for wide band applications. For each structure, properties of the vacuum waveguide mode are examined in connection with the gyrotron application, and the gyrotron dispersion relation is obtained. For the disk loaded gyrotron, it is found that the group velocity of the waveguide mode can be easily varied by the disk parameters, and the gain and the bandwidth are at least comparable to those of the ordinary gyrotron. In the helix waveguide configuration, the gyrotron utilizing the

DD FORM 1 JAN 73 1473 EDITION OF 1 NOV 65 IS OBSOLETE
S/N 0102-LF-014-6601

UNCLASSIFIED

SECURITY CLASSIFICATION OF THIS PAGE (When Data Entered)

helix mode can be very broad in its bandwidth. Moreover, the hybrid mode operation, using the helix mode as a carrier, shows possibility of fast wave wide band amplification by contouring waveguide.

FOREWORD

The gyrotron amplifiers in two slow wave structures, the disk and the helix loaded waveguides, are investigated for wide band applications. For each structure, properties of the vacuum waveguide mode are examined in connection with the gyrotron application, and the gyrotron dispersion relation is obtained. For the disk loaded gyrotron, it is found that the group velocity of the waveguide mode can be easily varied by the disk parameters, and the gain and the bandwidth are at least comparable to those of the ordinary gyrotron. In the helix waveguide configuration, the gyrotron utilizing the helix mode can be very broad in its bandwidth. Moreover, the hybrid mode operation, using the helix mode as a carrier, shows possibility of fast wave wide band amplification by contouring waveguide.

Approved by:

Ira M Blatstein

IRA M. BLATSTEIN, Head
Radiation Division

CONTENTS

ILLUSTRATIONS

I. INTRODUCTION

The gyrotron (Flyagin et al 1977, Hirschfield and Granatstein 1977) is a high power microwave tube that utilizes the fast wave coupling of the waveguide mode with the cyclotron frequency upshifted beam mode. One of the shortcomings of the gyrotron, however, is its narrow bandwidth, primarily due to the fast variation of the group velocity of the waveguide mode in a smooth wall configuration. Therefore, it is necessary to slow down the wave in order to broaden the bandwidth. In this regard, we have to re-examine various slow wave structures that have been widely used in conventional traveling wave tubes (Pierce 1950), in the context of the fast wave interaction of the gyrotron. In this paper we will examine the gyrotron in two of such slow wave structures; the periodic disk loaded gyrotron and the sheath helix loaded gyrotron. Another slow wave structure, the dielectric loaded gyrotron, has been exhaustively investigated already (Choe et al 1981).

Previous analyses of these two configurations exist (Chu and Hansen 1947, Walkinshaw 1948, Pierce 1950, Hutter 1950, Sensiper 1955), but these are limited to the slow wave applications to the TWT. In the periodic disk configuration the transverse magnetic (TM) mode is analyzed, and for the sheath helix waveguide most of them have ignored important role of the outer conducting wall. Here we will investigate the transverse electric (TE) mode suitable for the gyrotron interaction for the periodic disk geometry, and include the conducting wall in our analysis for the helix geometry to utilize the location of the wall as a useful parameter. The periodic disk loaded gyrotron will be discussed in Sec. II, and the sheath helix loaded gyrotron in Sec. III.

In view of the role that the vacuum waveguide mode plays in performance of the tubes, we will first examine the dispersion characteristics of the beam-free waveguide mode for each structure (in Subsection A). This will be followed by the

derivation of the gyrotron dispersion relation with the electron beam in Subsection B. For each structure, the Subsection B will include some numerical examples of the gyrotron gain. We emphasize that the objective of this paper is to examine the dispersion characteristics of the waveguide and to derive the gyrotron dispersion relation for two slow wave structures. Therefore, the detailed parametric optimization with respect to the gain and the bandwidth will be deferred for later works, only giving few typical examples.

II. DISK LOADED GYROTRON

We consider a cylindrical waveguide loaded with periodic disks as shown in Fig. 1. The thin disks extend radially from the outer conductor at $r = b$ to $r = a$ as shown, with the axial period given by L. The cylindrical coordinates (r,θ,z) are employed.

This configuration has been studied before in the context of the slow wave TWT interaction (Chu and Hansen 1947, Walkinshaw 1948). Thus these analyses have been limited to the TM modes. In order to utilize the same configuration for the fast wave interaction of the gyrotron, therefore, we must examine the TE modes. Otherwise the present analysis is similar to the previous ones. Emphases are, hence, on the differences between TM and TE modes. In Subsection A, the TE dispersion relation for the vacuum waveguide mode is obtained and discussed. The gyrotron dispersion relation with the electron beam is derived and an example of the gyrotron gain from this dispersion relation will be given in Subsection B.

A. Vacuum Waveguide Dispersion Relation

In this subsection we will derive and discuss the vacuum waveguide dispersion relation for the periodic disks shown in Fig. 1. We limit our attention to the azimuthally symmetric (i.e. $\partial/\partial\theta = 0$, $\ell = 0$) TE modes. Moreover, we will employ an approximate scheme in order to obtain an analytical result.

The procedure to obtain the approximate dispersion relation is given elsewhere (Choe and Uhm 1982), and only the outline will be given here. First, the domain is divided into two separate regions (I for $r \leq a$, II for $a \leq r \leq b$, see Fig. 1), and the electromagnetic fields for TE mode are expressed in the separate eigenfunction expansion for each region. The eigenfunctions are determined by the boundary conditions on the metalic boundaries and the axial periodic conditions (i.e. Floquet theorem, Slater 1950). Then, the dispersion relation results in by matching the fields at the mouth of the disks (i.e. at $r = a$), where an approximate method is used to simplify the dispersion relation.

The fields for each region (I and II) can be expressed as the sum of the space harmonic (n) waves in region I, and of the standing waves with the nodal number m for region II. Namely,

$$B_z^{I}(r,z) = \sum_{n=-\infty}^{\infty} C_n J_0(p_n r) \exp(ik_n z), \tag{1}$$

$$B_z^{II}(r,z) = \sum_{m=1}^{\infty} D_m \left[N_1(q_m b)\, J_0\, (q_m r) - J_1(q_m b)\, N_0\, (q_m r)\right] \times \sin(\kappa_m z), \tag{1'}$$

where

$$k_n \equiv k + 2n\pi/L, \qquad p_n^{\,2} \equiv \omega^2/c^2 - k_n^{\,2}, \tag{2}$$

$$\kappa_m \equiv m\pi/L, \qquad q_m^{\,2} \equiv \omega^2/c^2 - \kappa_m^{\,2}. \tag{2'}$$

Here ω and k refer to the frequency and the axial wavenumber, respectively, and J_ℓ and N_ℓ to the first and second kind of Bessel functions of order ℓ. Other TE components (E_θ, B_r) are given in terms of B_z. Here $\tilde{E}$ and $\tilde{B}$ denote the electric and magnetic fields. We note that the expression for E_z in TM mode is similar to eq. (1), with one notable exception. For TE mode the first term in region II is with m = 1, while it is with m = 0 for TM mode. The usual periodicity of the dispersion relation in the axial wavenumber k with the period of $2\pi/L$, and the symmetry with respect to k are evident from eq. (1), even without the field matching considerations. Thus it is sufficient to obtain the dispersion relation for $0 \leq k < \pi/L$.

Since an analytical dispersion relation is sought in this paper, we need an approximation scheme for matching fields at the mouth (r = a). Instead of matching fields for all z, we only match the average fields over the one axial

period L. That is, we demand that $<\psi^{I}> = <\psi^{II}>$, where ψ stands for the fields and $<\psi> = \int_0^L dz\ \psi(r = a,z)$. Furthermore, we assume that the axial wavenumber is small, that is,

$$kL << \pi. \tag{3}$$

Then it can be shown (Choe and Uhm 1982) that the dominant term is for n = 0 in region I and for m = 1 for region II, and that the average fields are matched provided eq. (3) is valid. This can be compared with TM mode where, with the same approximation scheme (eq. (3)), the n = 0 term in region I couples with the m = 0 term in region II. Within this truncation method, the dispersion relation for the TE mode is given by

$$D^{TE} = \psi_J\ (p_0a) - \phi_1(q_1b,q_1a) = 0\ , \tag{4}$$

where

$$\psi_J(x) \equiv J_1(x)/[xJ_0(x)],$$

$$\phi_i(y_b,y_a) \equiv \frac{N_i(y_b)J_1(y_a) - J_i(y_b)\ N_1(y_a)}{y_a\ [N_i(y_b)J_0(y_a) - J_i(y_b)N_0(y_a)]}\ . \tag{5}$$

We recall that the corresponding TM dispersion relation is given by $D^{TM} = \psi_J(p_0a) - \phi_0(q_0b,q_0a) = 0$. Here $p_n{}^2$ and $q_m{}^2$ are previously defined in eq. (2). The difference in the dominant term in region II (m = 1 for TE, m = 0 for TM) is reflected in the dispersion relation (ϕ_1 for TE, ϕ_0 for TM).

Careful examination of the dispersion relation reveals several characteristics of the disk loaded waveguide mode. For given k, the frequency ω is higher than that for the smooth wall (i.e. a = b). The reverse is true for the TM mode.

Also the frequency increases for given k as the period L decreases, and as the ratio a/b decreases. This can be compared with the TM mode, where ω is independent of L and increases as a approaches b (smooth wall). The lower cutoff frequency ω_{co} increases as L increases and as a/b decreases. For TM mode, ω_{co} is independent of both L and a/b. These dependence of the frequency on the period L and the ratio a/b are further illustrated in Fig. 2. In Fig. 2(a), the TE mode dispersion curves for several disk dimensions a/b are plotted at given period ($\pi b/L = 10.0$). It is evident from the graph the cutoff frequency ω_{co} at $k = 0$ is decreasing function of a/b. At the same time, if we extroplate our analysis to the limit at $k = \pi/L$, the frequencies for all a/b converge to that for the smooth wall. This pivot-like phenomenon occurs at $k = 0$ for the TM modes. Obviously the group velocity of the wave decreases as the ratio a/b decreases. The dependence on the period L is shown in Fig. 2(b). Here the dispersion curves are drawn for several L at given disk dimension ($a/b = 0.5$). Also shown is the dispersion curve for the smooth wall (broken curve) for reference. Evidently for given k, ω is an increasing function of L. The graph also reveals that the group velocity of the wave decreases as L increases. We conclude that the group velocity can be easily adjusted by variation of the disk parameters, a/b and L.

B. Gyrotron Dispersion Relation

In this subsection we will derive the dispersion relation for the disk loaded gyrotron in the presence of the electron beam. It is assumed that the thin hollow electron beam is located at $r = R_0 (0 < R_0 < a)$, under the influence of the strong axial magnetic field B_0, and the configuration otherwise is the same as in Fig. 1. Again we limit our attention to the azimuthally symmetric ($\ell = 0$) TE mode.

The analysis is carried out within the framework of the linearized Maxwell-Vlasov system for the fields $\underset{\sim}{E}$ and $\underset{\sim}{B}$, and for the beam electron distribution function f. Following the scheme in previous subsection, the perturbed fields are for those with the fundamental space harmonic (n = 0) and with the first nodal number (m = 1). Namely, in the vacuum region,

$$B_z = \begin{cases} A_1 J_0(p_0 r) , & 0 \le r \le R_0 , \\ A_2 J_0(p_0 r) + A_3 N_0(p_0 r) , & R_0 \le r \le a , \\ A_4 J_0(q_1 r) + A_5 N_0(q_1 r), & a \le r \le b . \end{cases} \tag{6}$$

The coefficients A's are to be determined from the boundary conditions, the field matching condition at r = a (Subsection A), and the jump condition on B_z at the beam location R_0. The jump condition on B_z at R_0, in turn, is obtained from the moment equation with the purturbed distribution function. In the present analysis we assume that the equilibrium distribution function f_0 is Lorentzian in the axial momentum p_z. Namely,

$$f_0 \propto \hat{p}_z \, \Delta / \left[(p_z - \hat{p}_z)^2 + \hat{p}_z^{\,2} \Delta^2 \right] , \tag{7}$$

where Δ refers to the axial momentum spread ratio. We further designate the total electron energy and the average axial (transverse) velocity by γmc^2 and $c\beta_z$ ($c\beta_\perp$), respectively. The jump condition at R_0, or equivalently impedance matching across the beam (Choe et al 1981), provides the dispersion relation for the gyrotron.

$$B = \frac{B_N}{B_D} = - \frac{\nu \beta_\perp^{\,2} c^2}{2\gamma R_0^{\,2} \left[\omega - \omega_B + ic|k|\beta_z \gamma \Delta / \gamma_z^{\,3} \right]^2} \tag{8}$$

where

$$B_N = 2B_1 \quad B_D = -\pi x_0^2 J_1(x_0) \left[J_1(x_0)\, B_2 - N_1(x_0)\, B_1\right] ,$$

$$B_1 = J_0(x_a) \left[\psi_J(x_a) - \phi_1\, (y_b, y_a)\right] ,$$

$$B_2 = N_0(x_a) \left[\psi_N(x_a) - \phi_1\, (y_b, y_a)\right] ,$$

$$\begin{Bmatrix} x_a^2 \\ x_0^2 \end{Bmatrix} = p_0^2 \begin{Bmatrix} a^2 \\ R_0^2 \end{Bmatrix} , \quad \begin{Bmatrix} y_b^2 \\ y_a^2 \end{Bmatrix} = q_1^2 \begin{Bmatrix} b^2 \\ a^2 \end{Bmatrix} , \tag{9}$$

$$\psi_N(x) \equiv N_1(x)/\left[x\, N_0(x)\right] ,$$

$$\omega_B = kc\beta_z + \omega_c/\gamma, \quad \gamma_z = \left(1 - \beta_z^2\right)^{-1/2} ,$$

and $\omega_c = eB_0/mc$ is the non-relativistic cyclotron frequency and $\nu \equiv Ne^2/mc^2$ is the Budker parameter. Here N is the total number of electrons per unit axial length, c is the velocity of light, and (-e) and m are the electronic charge and mass. The quantities, p_0, q_1, ψ_J, ϕ_1, and Δ are previously defined in eqs. (2), (5) and (7). Note that $B_1 \propto D^{TE}$ so that the equation (8) recovers the vacuum waveguide dispersion relation (4) when the beam is absent ($\nu = 0$). The dispersion relation (8) can be used to investigate gain and bandwidth of the disk loaded gyrotron amplifier for a broad range of physical parameters. Here we will give only one example in Fig. 3. At the given system parameters ($\nu = 0.002$, $\beta_\perp = 0.4$, $\beta_z = 0.2$, $a/b = 0.3$, $a\omega_c/c = 2.8$, $L\, \omega_c/c = 3.2$, $R_0\, \omega_c/c = 2.0$), the normalized gain ($-100\, k_i\, c/\omega_c$) versus the normalized frequency (ω/ω_c) is plotted for several values of the axial velocity spread (Δ). Even without the benefit of the parametric optimization, both the gain and the bandwidth for this disk loaded gyrotron are at least comparable to those for the smooth wall gyrotron. We will leave the parametric optimization as future works.

III. HELIX LOADED GYROTRON

As illustrated in Fig. 4, the system configuration consists of a sheath helix with radius R_h located inside a cylindrical conductor at R_c. We assume that conducting wires in the helix are very fine in texture, thereby replacing the actual helix by a helically conducting sheet. This sheet is perfectly conducting in a helical direction making a pitch angle ϕ with a plane normal to the axis of the system, as shown in Fig. 4. The effect of the helix is then restricting the current over the sheet in ϕ direction, while allowing the fields penetration to $R_h > r > R_c$. Again the cylindrical coordinates are used.

Although this helix structure has been investigated before (Pierce 1950, Sensiper 1955, Berezin et al 1960), these studies either neglect the role of the outer conductor, thereby restricting to slow wave propagation only, or concentrate only on the azimuthally symmetric ($\ell=0$) mode. We, therefore, investigate the dispersion characteristics for arbitrary azimuthal mode number ($\ell \neq 0$) including the outer conductor. As before, the vacuum waveguide dispersion relation is obtained and analyzed in subsection A. Two interesting limits, namely as $R_c \rightarrow \infty$ and as $R_c \rightarrow R_h$, are examined. The former recovers previous results and the latter yields clear pictures of the mode identifications. The gyrotron dispersion relation with the electron beam will be derived and some numerical examples will be given in subsection B.

A. Vacuum Waveguide Dispersion Relation

Since the detailed procedure of the vacuum dispersion relation is given elsewhere (Uhm and Choe 1982a), only the brief outline will be given

here. In anticipation of the presence of the hybrid modes, we express both E_z and B_z as a general solution of the wave equation for the Fourier component ℓ (azimuthal mode number), k (axial wavenumber) and ω (frequency). Then the boundary conditions on the wall and on the helix yield the desired dispersion relation.

The primary fields E_z and B_z are given by

$$E_z = \begin{cases} A_1^E \; J_\ell(pr) & 0 \le r \le R_h \\ A_2^E \left[N_\ell(pR_c)\, J_\ell(pr) - J_\ell(pR_c)\, N_\ell(pr) \right], & R_h \le r \le R_c \end{cases} \tag{10}$$

$$B_z = \begin{cases} A_1^B \; J_\ell(pr), & 0 \le r < R_h \\ A_2^B \left[N_\ell'(pR_c)\, J_\ell(pr) - J_\ell'(pR_c)\, N_\ell(pr) \right], & R_h < r \le R_c \end{cases}$$

where

$$p^2 \equiv \omega^2/c^2 - k^2, \tag{11}$$

and the prime (´) denotes the derivative of Bessel functions. Other components of the fields are given in terms of E_z and B_z. The boundary conditions on the sheath helix ($r=R_h$) are

$$\begin{aligned} &\underset{\sim}{E} \cdot \hat{e}_\phi \Big|_{R_h^\pm} = 0 \,, \\ &\underset{\sim}{E} \times \hat{e}_\phi \Big|_{R_h^-} = \underset{\sim}{E} \times \hat{e}_\phi \Big|_{R_h^+} \\ &\underset{\sim}{B} \cdot \hat{e}_\phi \Big|_{R_h^-} = \underset{\sim}{B} \cdot \hat{e}_\phi \Big|_{R_h^+} \end{aligned} \tag{12}$$

where $\hat{e}_\phi$ is the unit vector in the helix direction ϕ, and $R_h^{\pm}$ refers to the evaluation at just inside (-) or just outside (+) the helix surface. The dispersion relation for the vacuum waveguide mode is obtained by combining eqs. (10) and (12). The resultant dispersion relation is given by

$$D = \frac{\omega^2}{c^2} R_h^2 \, J_\ell(X_c) J_\ell'(X_h) + X_h^2 \, t_\ell^2 J_\ell'(X_c) J_\ell(X_h) f = 0 \qquad (13)$$

where

$$f = f_N/f_D, \quad t_\ell = \tan\phi - \ell k R_h / X_h^{\,2},$$

$$f_N = J_\ell(X_c) N_\ell(X_h) - N_\ell(X_c) J_\ell(X_h),$$

$$f_D = J_\ell'(X_c) N_\ell'(X_h) - N_\ell'(X_c) J_\ell'(X_h), \qquad (14)$$

$$\begin{Bmatrix} X_h^{\,2} \\ X_c^{\,2} \end{Bmatrix} = p^2 \begin{Bmatrix} R_h^{\,2} \\ R_c^{\,2} \end{Bmatrix},$$

and p^2 is defined in eq. (11). Note that the sign of p^2 determines whether the wave is fast ($\omega > ck$, $p^2 > 0$) or slow ($\omega < ck$, $p^2 < 0$).

In the limit $R_c \to \infty$, the dispersion relation (13) is further simplified as

$$\frac{\omega^2}{c^2} = - p^2 t_\ell^{\,2} \frac{J_\ell(X_h) N_\ell(X_h)}{J_\ell'(X_h) N_\ell'(X_h)}, \qquad (15)$$

which has solutions only when $p^2 < 0$. This means that when the outer conductor is removed, only the slow wave ($\omega < ck$) can propagate. The dispersion relation (15) with Bessel functions J and N explicitly given by modified functions I and K

can be found in previous literatures (Pierce 1950, Hutter 1950, Sensiper 1955). More interesting features can be found in the other limit. Namely, on the limiting case when the outer conductor approaches to the helix (i.e. $R_c \to R_h$), eq. (13) is reduced to

$$J_\ell'(X_c)\, J_\ell(X_c) \left\{ \frac{\omega^2}{c^2} - \left[k \sin\phi + (\ell/R_c) \cos\phi \right]^2 \right\} = 0. \tag{16}$$

From eq. (16), we identify three distinctive solutions; the transverse electric (TE) mode

$$\frac{\omega^2}{c^2} - k^2 = \frac{\alpha_{\ell s}{}^2}{R_c{}^2}, \tag{17}$$

the transverse magnetic (TM) mode

$$\frac{\omega^2}{c^2} - k^2 = \frac{\beta_{\ell s}{}^2}{R_c{}^2}, \tag{18}$$

and the helix mode

$$\omega = \pm \left[ck \sin\phi + \ell(c/R_c) \cos\phi \right], \tag{19}$$

where $\alpha_{\ell s}$ and $\beta_{\ell s}$ are the Sth roots of $J_\ell'(\alpha_{\ell s}) = 0$ and $J_\ell(\beta_{\ell s}) = 0$, respectively.

It is remarkable to note from eq. (19) that the helix mode for $R_c \to R_h$ is a straight line in the (ω, k) space. Thus, when the helix mode with $R_h/R_c \to 1$ is coupled with the electron beam mode ($\omega_B = kc\beta_z + \omega_c/\gamma$, eq. (9)) for the gyrotron, a super wide band amplifier can be constructed by a choice of appropriate beam parameters satisfying

$$\beta_z \simeq \sin\phi, \qquad R_c \simeq \gamma c \ell \cos\phi/\omega_c. \tag{20}$$

In general case where $R_c/R_h \neq 1$, there exist two distinguishing kinds of modes; (a) the hybrid waves mainly consisting of a combination of the TE and TM modes and (b) the helix mode. The dispersion relation (14) is numerically solved for ω at given k. Shown in Fig. (5) are plots of the normalized frequency $\omega R_c/c$ versus the normalized wavenumber kR_c obtained from eq. (14) for the helix mode, $\phi = \pi/6$, (a) $R_c/R_h = 1.43$ and several values of ℓ and (b) $\ell = 2$ and several values of R_c/R_h. We note from Fig. 5(a) that for the $\ell \neq 0$ helix mode, the dispersion curve for the slow wave region ($\omega < ck$) is continuously connected to that for a portion of fast wave region ($\omega > ck$). On the other hand, the dispersion curve for the $\ell = 0$ helix mode consists entirely of the slow wave region. As mentioned above, the dispersion curves of the helix mode in Fig. 5(b) approach to the straight lines described by eq. (19) as the parameter R_c/R_h decreases to unity.

As expected, there are infinite number of the hybrid waves which are identified by the radial node number n. All of these hybrid modes are fast waves ($\omega > ck$). Figure 6 is the plot of the frequency versus the wavenumber obtained from eq. (14) for the n = 1 hybrid waves, $\phi = \pi/6$, $R_c/R_h = 1.43$, and several values of ℓ. Note that the dispersion curves for the $\ell \neq 0$ hybrid waves is not symmetric about k = 0 line. Additional information on the vacuum dispersion properties are given in our previous paper (Uhm and Choe 1982a).

B. Gyrotron Dispersion Relation

The dispersion relation for the helix loaded gyrotron in the presence of the electron beam will be derived in this subsection. The thin hollow electron beam, located at $r = R_0$ $(0 < R_0 < R_h)$, is assumed to be embedded in the strong axial magnetic field B_0. The system configuration is otherwise same as given in Fig. 4.

The detailed derivation of the dispersion is given elsewhere (Uhm and Choe 1982b). The general procedure is similar to that given in Sec. II B. Within the framework of the linearized Maxwell-Vlasov system, the perturbed fields in the vacuum region are given as general solutions of the wave equation similar to eq. (10), and the boundary condition on the helix (eq. (12)) and the jump condition on B_z across the beam location yields the dispersion relation. The jump condition is given by the moment equation of the perturbed distribution function, which is computed from the equilibrium distribution function given by eq. (7).

Then we finally obtain the dispersion relation for the Fourier component ℓ (azimuthal), k (axial wavenumber), and ω (frequency) in the helix loaded waveguide.

$$B = \frac{B_N}{B_D} = - \frac{\nu \beta_I{}^2 c^2}{2\gamma R_0{}^2 \left[\omega - \omega_B + ic|k|\beta_z \gamma \Delta/\gamma_z{}^3\right]^2}, \qquad (21)$$

where

$$B_N = 2B_1, \quad B_D = -\pi X_0{}^2 J_{\ell-1}(X_0)\left[J_{\ell-1}(X_0)B_2 - N_{\ell-1}(X_0)B_1\right].$$

$$B_1 = \frac{\omega^2}{c^2} R_h{}^2 J_\ell(X_c) J_\ell'(X_h) f_D + X_h{}^2 t_\ell{}^2 J_\ell'(X_c) J_\ell(X_h) f_N,$$

$$B_2 = \frac{\omega^2}{c^2} R_h{}^2 J_\ell(X_c) N_\ell'(X_h) f_D + X_h{}^2 t_\ell{}^2 N_\ell'(X_c) J_\ell(X_h) f_N \qquad (22)$$

$$- k R_h X_h t_\ell f_D f_N,$$

$$X_0{}^2 = p^2 R_0{}^2.$$

Here the quantities, X_h, X_c, f_D, f_N, t_ℓ and p^2 are defined in eqs. (14) and (11). The beam mode ω_B is defined in eq. (9) and the axial velocity spread ratio Δ appears in eq. (7). We note that in the limit of $\nu \to 0$, the dispersion relation (21) recovers the vacuum waveguide dispersion equation (13) (i.e. $B_I \propto D$). The dispersion relation in eq. (21) can be used to investigate gain and the bandwidth of the helix loaded gyrotron amplifier for a broad range of physical parameters.

In the remainder of this subsection we show several numerical examples of the gyrotron gain (k_i) versus the frequency with assumed beam parameters, ν=0.002, $\beta_\perp$ = 0.4, β_z = 0.2. In order to illustrate the broad band amplification in a helix loaded waveguide, Fig. 7 shows a plot of the normalized gain ($-100k_ic/\omega_c$) versus the normalized frequency ω/ω_c obtained from eq. (21) for the helix mode, Δ = 2%, R_c/R_h = 1.1, $R_0 = R_h - r_L$, and optimum values of the parameters ($R_h\omega_c/c, \phi$) for each azimuthal harmonic number ℓ. The optimum values of the parameters ($R_h\omega_c/c, \phi$) are given by (1.04, 10.6°) for ℓ = 1, (2.09, 11.0°) for ℓ = 2, (3.15, 11.0°) for ℓ = 3 and (4.21, 11.0°) for ℓ = 4. The normalized electron Larmor radius is $r_L\omega_c/c$ = 0.447. As expected in previous subsection, utilizing the helix mode for $R_h/R_c \simeq 1$, it is shown that a super wide band gyrotron amplifier is attainable for $\beta_z \simeq \sin\phi$ and $R_c \simeq \gamma c\ell \cos\phi / \omega_c$ (eq. (20)). For example, for ℓ = 2 and Δ = 2% in Fig. 7, the amplifier bandwidth is more than 60%. Here, the bandwidth is defined by the full width of the real frequency, at which the linear gain drops to exp (-1/2) of its maximum value, normalized by the mean frequency. When the axial velocity spread Δ is increased, the gain and bandwidth are considerably reduced. However, for ℓ = 2, the bandwidth of the gyrotron amplifier is found to be still more than 40% for Δ = 4%. We can conclude, therefore, the helix mode amplifier is a very effective means to amplify a broad band microwave signal.

In addition to the helix mode, the fast hybrid mode can be used for the gyrotron amplifier. As a typical example of the hybrid wave utilization, Fig. 8 presents plots of the gain versus the frequency for $\ell = 0$, $n = 1$, $R_0 = R_h - r_L$, and the geometric parameters $R_c/R_h = 1.5$, $R_h\omega_c/c = 2.25$ and $\phi = -60^\circ$, which satisfy the grazing condition. Also shown in the horizontal line is $k_b c/\omega_c = \omega/\omega_c - 1/\gamma$. Although the vacuum waveguide mode for $(\ell,n) = (0,1)$ is orginated from the TM mode, the maximum gain in Fig. 8 is very similar to that for the ordinary gyrotron where the beam mode couples with the TE mode. This strongly indicates that the hybrid wave for $(\ell,s) =$ (0,1) TE and TM modes in eqs. (17) and (18). The fast wave wide band amplification (Lau and Chu 1981) in a helix loaded waveguide is currently under investigation by authors, utilizing these hybrid waves as an amplification mechanism and the helix mode as a signal carrier. The general behavior of the gyrotron gain remains the same for the hybrid modes with $\ell \neq 0$.

IV. CONCLUSION

In this paper we have investigated the gyrotron amplifiers in a disk and a helix loaded waveguides. For each slow wave structure, the vacuum waveguide mode is derived and analyzed, and the gyrotron dispersion relation is obtained.

The disk loaded waveguide is discussed in Sec. II. The dispersion characteristics of the azimuthally symmetric TE mode are examined and compared with those of the TM mode in Sec. IIA. It has been found that the low cutoff frequency of the disk loaded TE mode is higher than that for the smooth wall, and that the group velocity of the wave can be easily adjusted by disk parameters. In Sec. IIB, the gyrotron dispersion relation in the disk configuration is obtained and a numerical example of the gain is given. The gain and the bandwidth of the disk loaded gyrotron is at least comparable to those for the smooth wall gyrotron.

In Sec. III, the helix loaded gyrotron is examined. The analysis of the vacuum waveguide mode reveals that the helix configuration supports two distinctive modes; the fast wave hybrid modes and the helix mode. In particular, when the outer conductor is very close to the helix, the helix mode becomes a straight line in the dispersion (ω,k) space. From Sec. IIB, it is shown that, by proper choice of the helix parameters, the bandwidth of the gyrotron utilizing the helix mode can be very wide, in excess of 40% even for 4% of the velocity spread. Also, by coupling with the hybrid mode and using the helix wave as a signal carrier, the hybrid mode gyrotron can be used as one of fast wave wide band schemes.

V. ACKNOWLEDGEMENT

This research was supported by the Independent Research Fund at the Naval Surface Weapons Center.

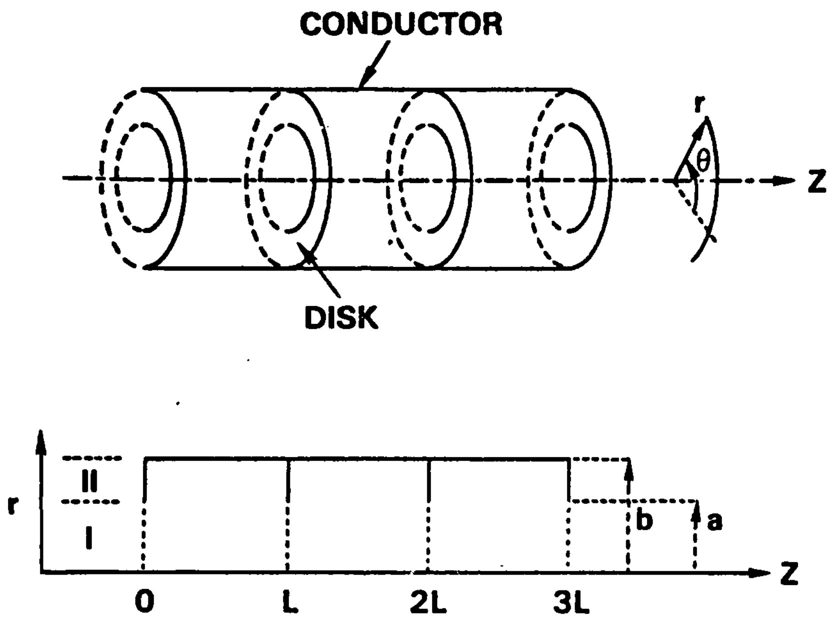

FIGURE 1. SYSTEM CONFIGURATION OF A DISK LOADED WAVEGUIDE

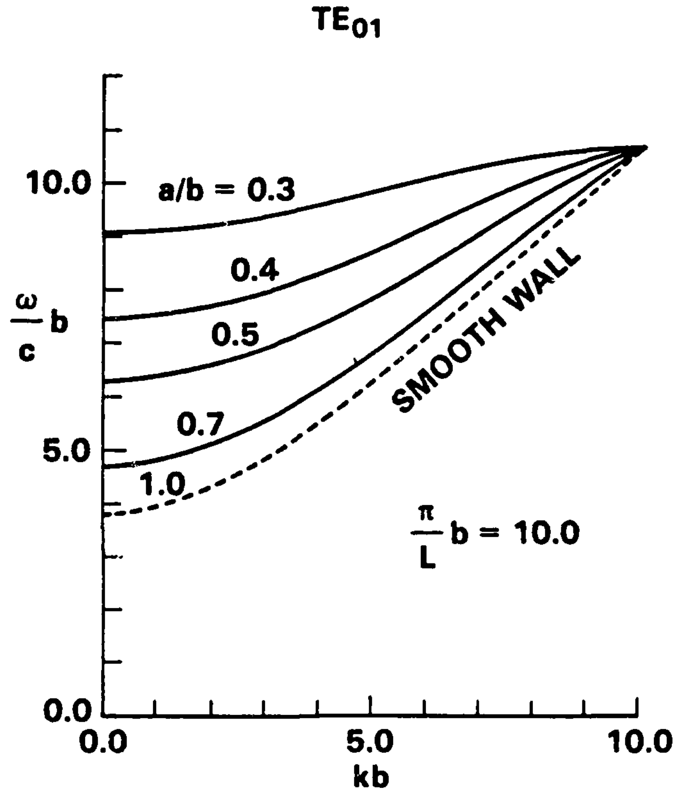

FIGURE 2A. DEPENDENCE OF THE DISPERSION ON THE DISK GEOMETRY (A/B)

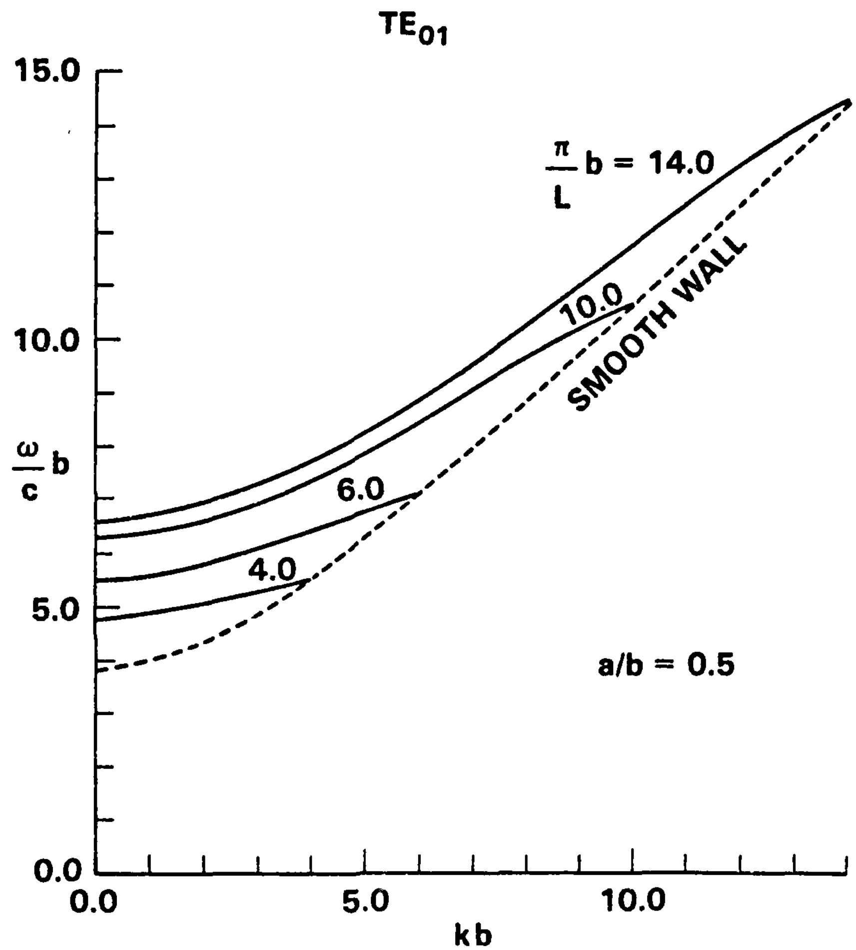

FIGURE 2B. DEPENDENCE OF THE DISPERSION ON THE PERIOD (L)

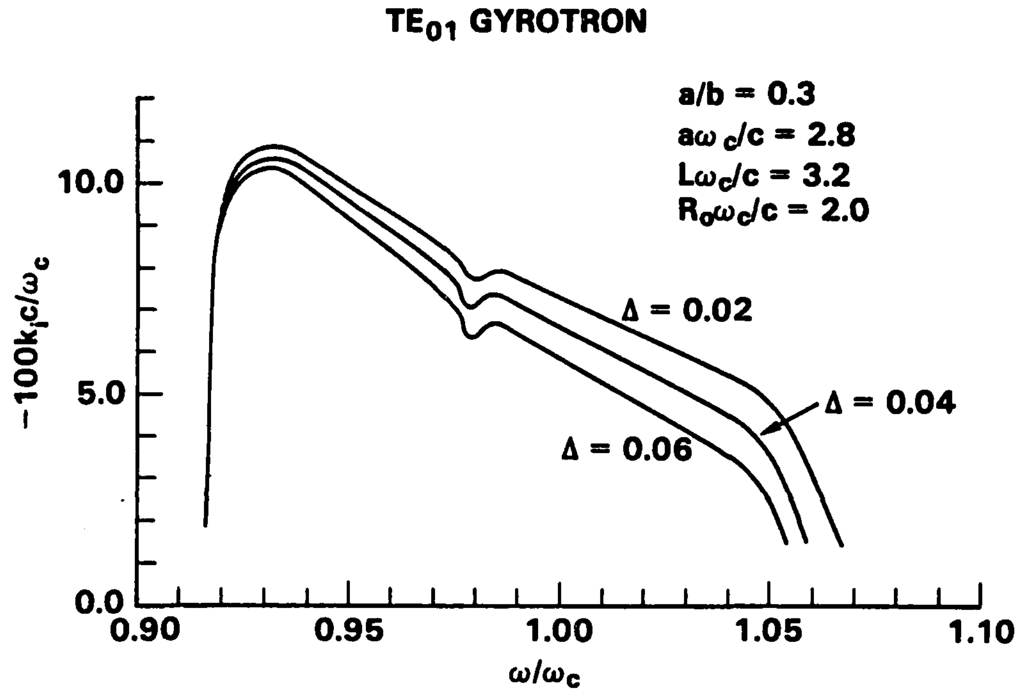

FIGURE 3. AN EXAMPLE OF THE DISK LOADED GYROTRON AMPLIFIER. THE NORMALIZED GAIN ($-100\ k_i c/\omega_c$) FOR SEVERAL VALUES OF THE AXIAL VELOCITY SPREAD (Δ) IS PLOTTED AGAINST THE NORMALIZED FREQUENCY (ω/ω_c)

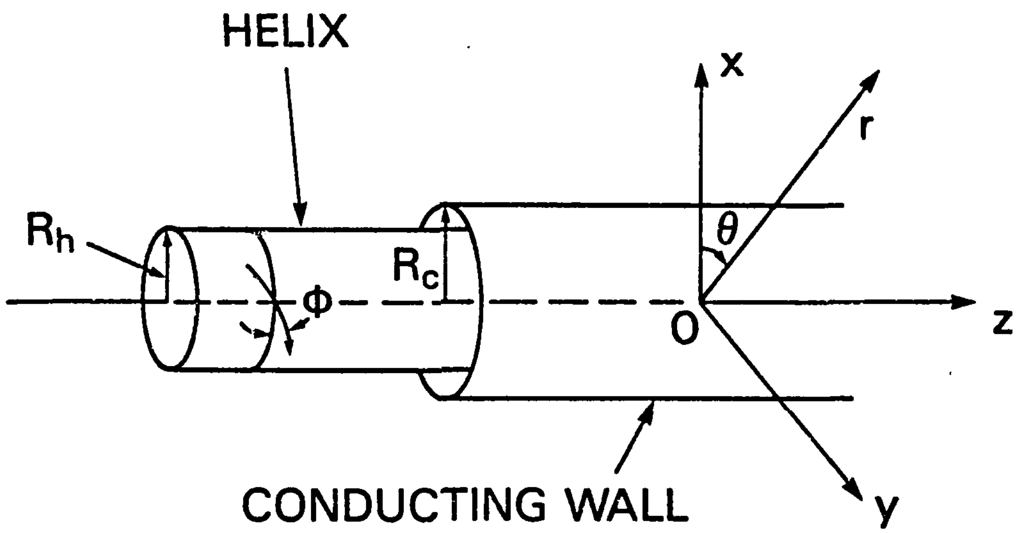

FIGURE 4. SYSTEM CONFIGURATION OF A SHEATH HELIX LOADED WAVEGUIDE

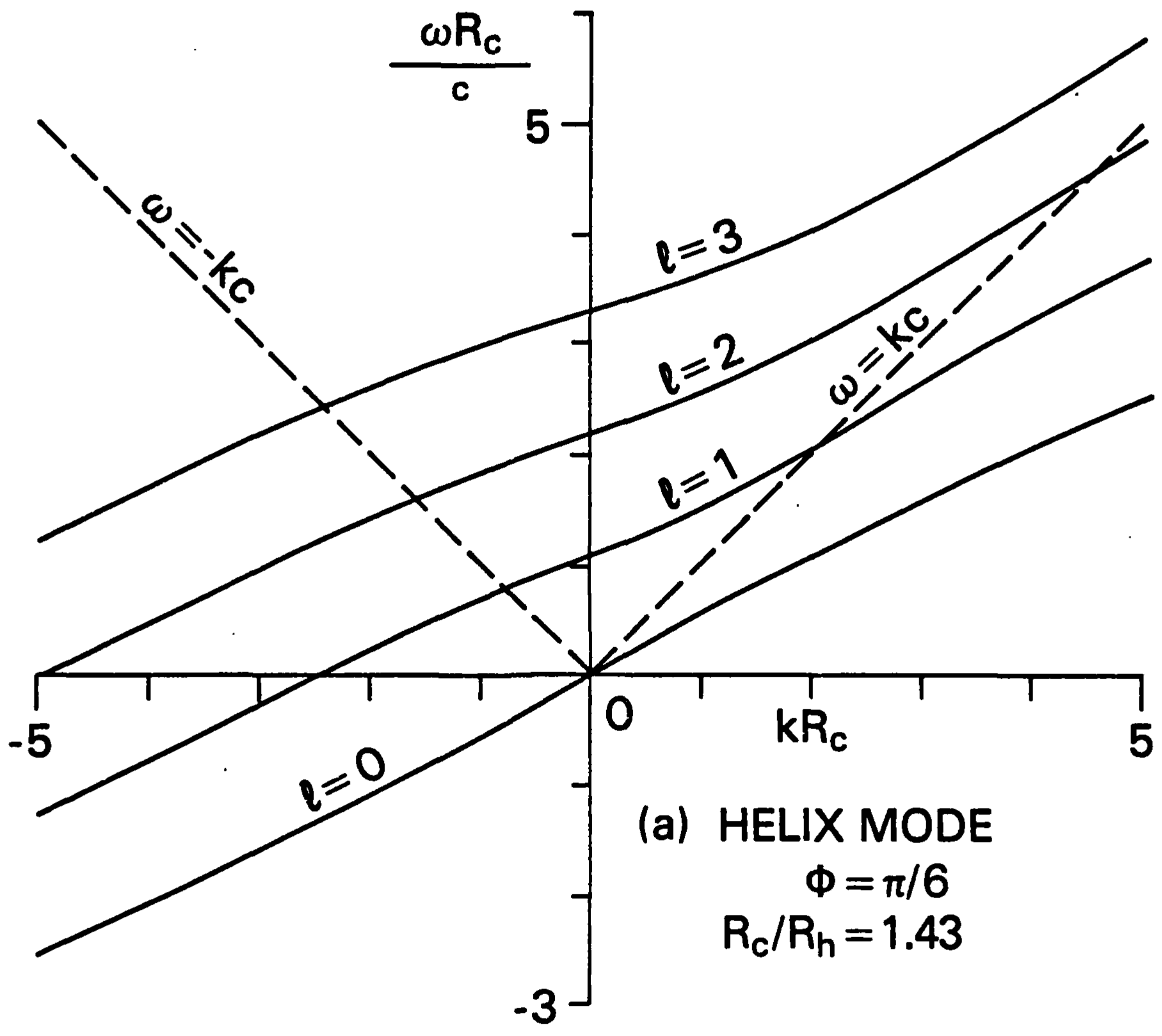

FIGURE 5A. PLOTS OF DISPERSION CURVES FOR THE HELIX MODES WITH $\phi = \pi/6$, $R_0/R_h = 1.43$ FOR SEVERAL VALUES OF ℓ

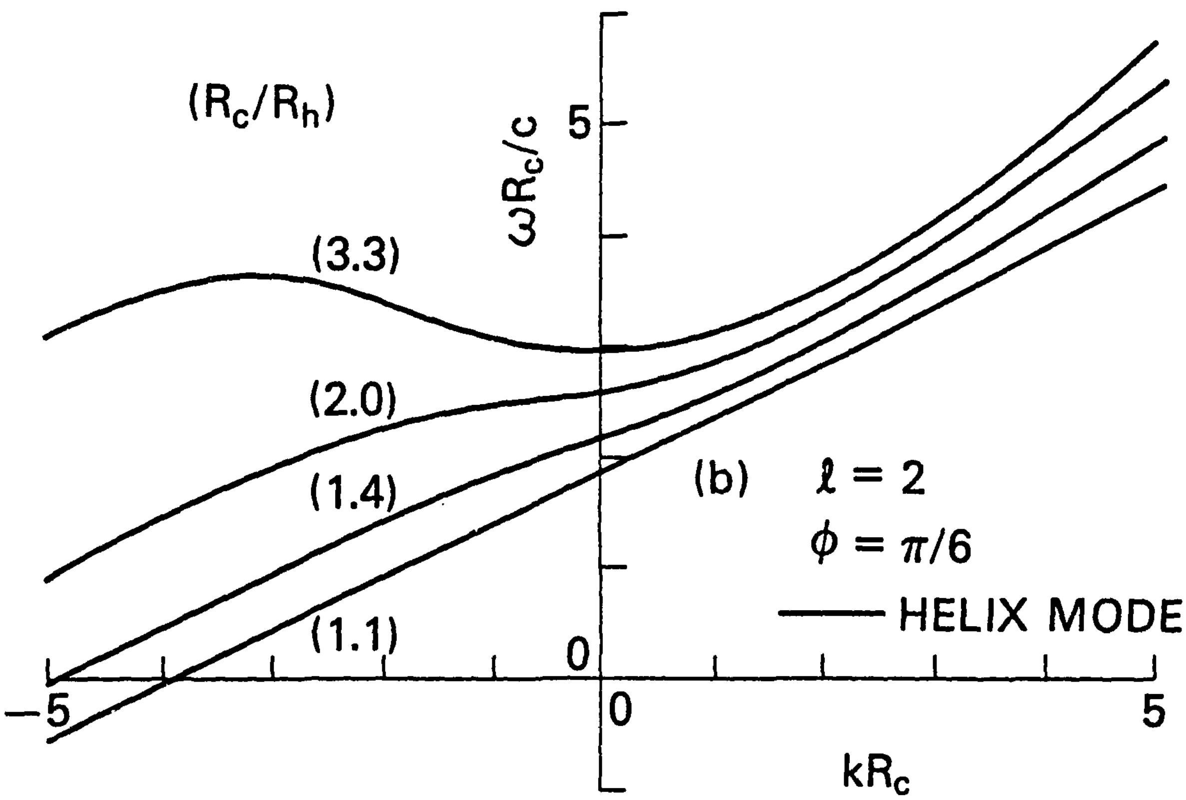

FIGURE 5B. PLOTS OF DISPERSION CURVES FOR THE HELIX MODES WITH $\phi = \pi/6$, $\ell = 2$ FOR SEVERAL VALUES OF R_c/R_h

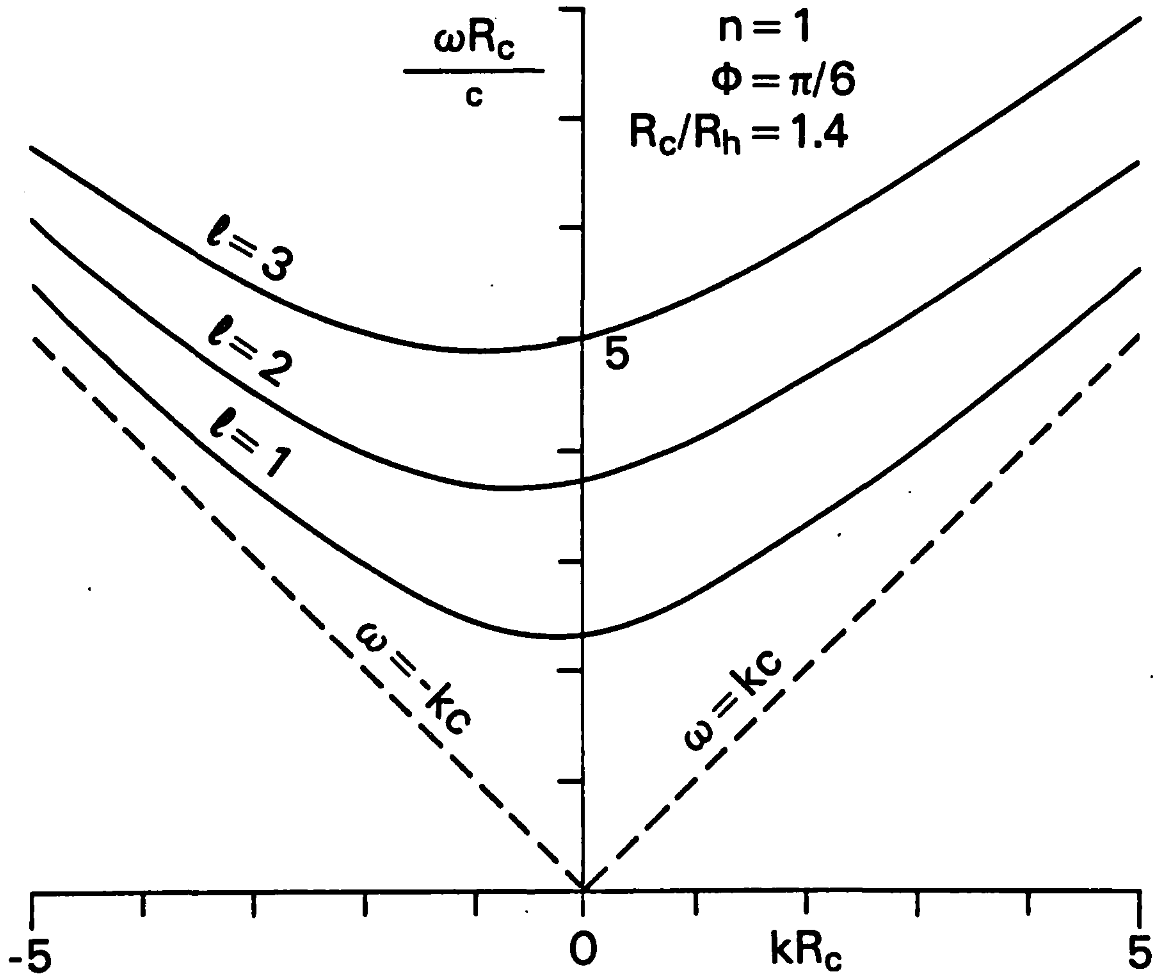

FIGURE 6. PLOTS OF DISPERSION CURVES FOR THE n = 1 HYBRID MODES WITH $\phi = \pi/6$, $R_c/R_h = 1.4$ FOR SEVERAL VALUES OF ℓ

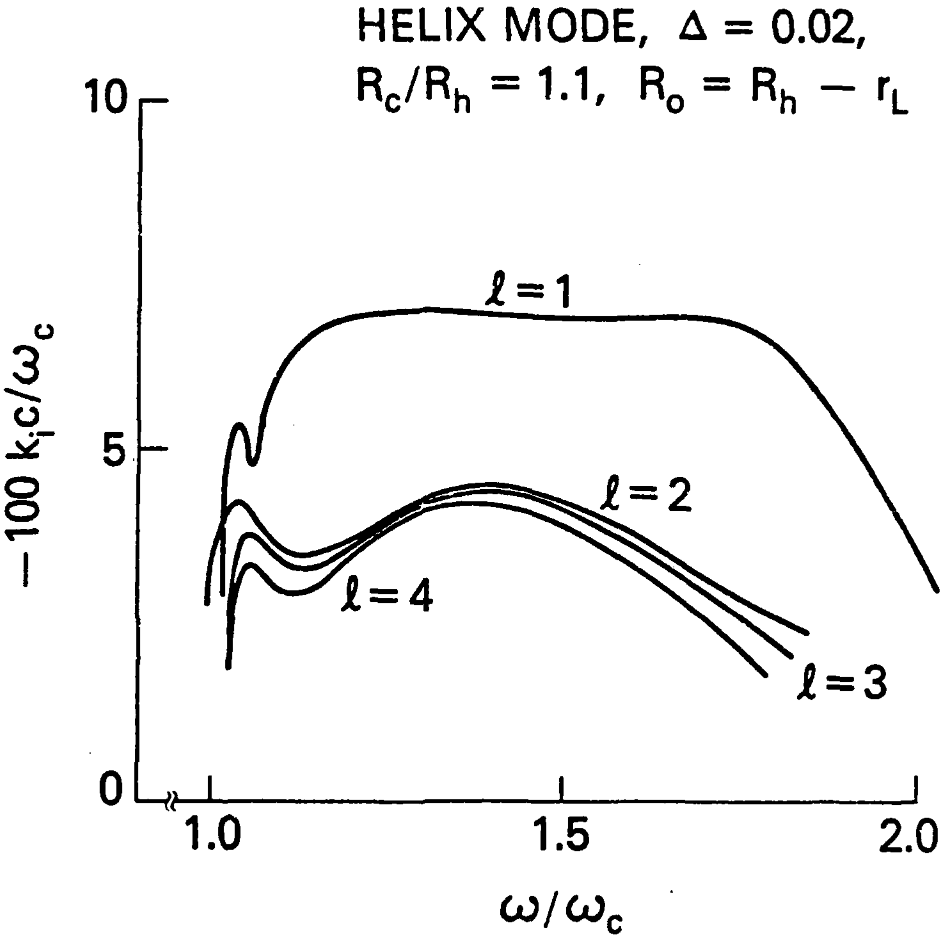

FIGURE 7. PLOTS OF THE GAIN VERSUS THE FREQUENCY FOR THE HELIX MODE WITH $\Delta = 2\%$, $R_c/R_h = 1.1$, $R_0 = R_h - r_L$ FOR SEVERAL VALUES OF ℓ

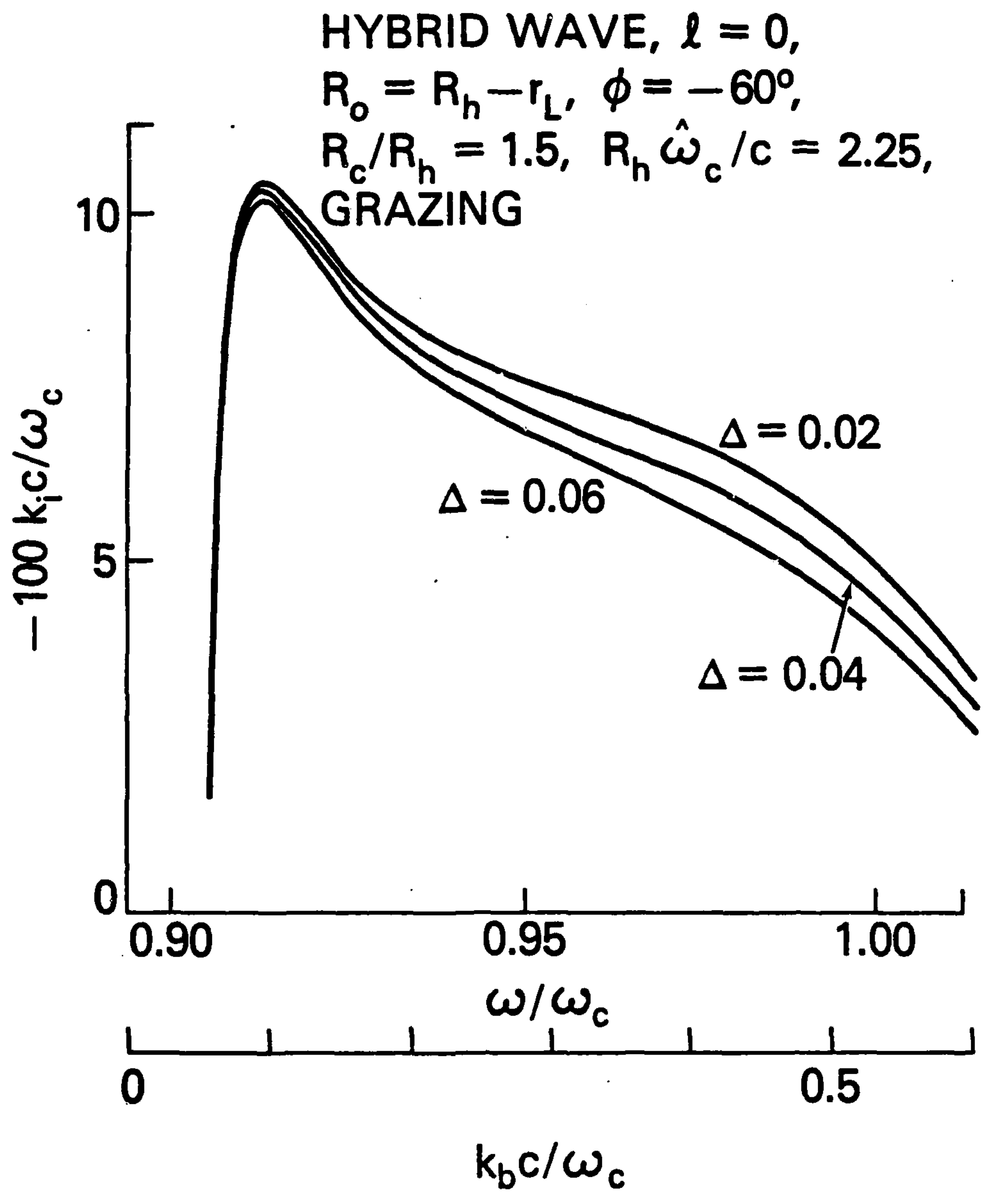

FIGURE 8. PLOTS OF THE GAIN VERSUS THE FREQUENCY FOR THE n = 1 HYBRID WAVE WITH $\ell = 0$, $R_0 = R_h - r_L$, $\phi = -60°$, $R_c/R_h = 1.5$, $R_h\ \omega_c/c = 2.25$ FOR SEVERAL VALUES OF Δ

BIBLIOGRAPHY

Berezin, A. K., Zeidlits, P. M., Nekhrshevich, A. M., and Silenok, G. A., 1960, Soviet Phys. Tech. Phys., 4, 730.

Choe, J. Y., and Uhm, H. S., 1982, IEEE Int'l. Conf. on Plasma Science, Conf. Rec., 62.

Choe, J. Y., Uhm, H. S., and Ahn, S., 1981, J. Appl. Phys., 52, 4508; and references therein.

Chu, E. L., and Hansen, W. W., 1947, J. Appl. Phys., 18, 996.

Flyagin, V. A., Gaponov, A. V., Petelin, M. I., and Yulpatov, V. K., 1977, IEEE Microwave Theory Tech., MTT-25, 514; and references therein.

Hirschfield, J. L., and Granatstein, V. L., 1977, IEEE Microwave Theory Tech., MTT-25, 528; and references therein.

Hutter, R. E. G., 1960, Beam and Wave Electronics in Microwave Tubes, Van Nostrand, New York.

Lau, Y. Y., and Chu, K. R., 1981, Int'l. J. Infrared and Millimeter Wave, 2, 415.

Pierce, J. R., 1950, Traveling-Wave Tubes, Van Nostrand, New York.

Sensiper, S., 1955, Proc. IRE, 43, 149.

Slater, J. C., 1950, Microwave Electronics, Van Nostrand, New York.

Uhm, H. S., and Choe, J. Y., 1982a, Properties of the electromagnetic wave propagation in a helix loaded waveguide (submitted for publication); 1982b, Gyrotron amplifier in a helix loaded waveguide (submitted for publication).

DISTRIBUTION

	Copies		Copies
Dr. Richard E. Aamodt Science Applica:ion Inc. 934 Pearl St. Suite A Boulder, CO 80302	1	Dr. J. Bayless DARPA Attn: DEO 1400 Wilson Blvd. Arlington, VA 22209	1
Dr. Saeyoung Ahn Code 5205 Naval Research Lab. Washington, D.C. 20375	1	Dr. Robert Behringer ONR 1030 E. Green Pasadena, CA 91106	1
Dr. Wahab A. Ali Naval Research Lab. Code 4700 4555 Overlook Ave., S.W. Washington, D.C. 20375	1	Prof. George Bekefi Bldg. 36-213, MIT 77 Massachusetts Ave. Cambridge, MA 02139	1
Dr. Donald Arnush TRW, Plasma Physics Dept. R1/107 1 Space Park Rodondo Beach, CA 90278	1	Dr. Gregory Benford Physics Department University of California Irvine, CA 92717	1
Dr. J.M. Baird Code 4740 (B-K Dynamics) Naval Research Lab. 4555 Overlook Ave., S.W. Washington, D.C. 20375	1	Dr. Jim Benford Physics International Co. 2700 Merced St. San Leandro, CA 94577	1
Dr. William A. Barletta Lawrence Livermore National Lab. L-321 University of California Livermore, CA 94550	1	Dr. Kenneth D. Bergeron Plasma Theory Div. - 5241 Sandia Laboratories Albuquerque, NM 87115	1
Dr. L. Barnett Code 4740 (B-K Dynamics) Naval Research Lab. 4555 Overlook Ave., S.W. Washington, D.C. 20375	1	Dr. T. Berlincourt Office of Naval Research Department of the Navy Arlington, VA 22217	1

DISTRIBUTION (Cont.)

	Copies
Dr. I. B. Bernstein Yale University Mason Laboratory 400 Temple Street New Haven, CT 06520	1
Dr. O. Book Code 4040 Naval Research Laboratory Washington, D.C. 20375	1
Dr. Jay Boris Naval Research Lab. Code 4040 4555 Overlook Ave., S.W. Washington, D.C. 20375	1
Dr. Howard E. Brandt Harry Diamond Labs 2800 Powder Mill Road Adelph, MD 20783	1
Dr. R. Briggs Lawrence Livermore Lab. P.O. Box 808 Livermore, CA 94550	1
Dr. K. Brueckner La Jolla Institute P.O. Box 1434 La Jolla, CA 92038	1
Dr. Herbert L. Buchanan Lawrence Livermore National Lab L-321 University of California Livermore, CA 94550	1
Dr. K. J. Button Massachusetts Institute of Technology Francis Bitter National Magnet Laboratory Cambridge, MA 02139	1
Dr. Neal Carron Mission Research Corp. 735 State Street Santa Barbara, CA 93102	1
Dr. Frank Chambers Lawrence Livermore National Lab. L-321 University of California Livermore, CA 94550	1
Prof. F. Chen Dept. of E. E. UCLA Los Angeles, CA 90024	1
Dr. M. Caponi TRW Advance Tech. Lab. 1 Space Park Redondo Beach, CA 90278	1
Dr. K. R. Chu Naval Research Lab. Code 4740 4555 Overlook Ave., S.W. Washington, D.C. 20375	1
Dr. Timothy Coffey Naval Research Lab. 4555 Overlook Ave., S.W. Washington, D.C. 20375	1
Dr. W. J. Condell Office of Naval Research Code 421 Department of the Navy Arlington, VA 22217	1
Dr. G. Cooperstein Naval Research Lab. Washington, D.C. 20375	1
Dr. Edward Cornet W.J. Schafer Associates, Inc. 1901 North Fort Myer Dr. Arlington, VA 22209	1

DISTRIBUTION (Cont.)

	Copies
Prof. R. Davidson Plasma Fusion Center Massachusetts Inst. of Technology Cambridge, MA 02139	1
Dr. J. Dawson Dept. of Physics UCLA Los Angeles, CA 90024	1
Dr. W. Destlar Dept. of Electrical Engineering University of Maryland College Park, MD 20742	1
Prof. P. Diament Columbia University Dept. of Electrical Engineering New York, NY 10027	1
Prof. W. Doggett NC State University P.O. Box 5342 Raleigh, NC 27650	1
Dr. H. Dreicer Plasma Physics Division Los Alamos Scientific Lab. Los Alamos, NM 87544	1
Dr. A. Drobot Naval Research Laboratory Code 4790 (SAI) Washington, D.C. 30275	1
Prof. W. E. Drummond Austin Research Associates 1901 Rutland Drive Austin, TX 78758	1
Prof. H. H. Fleischmann Lab. for Plasma Studies and School of Applied and Engr. Physics Cornell University Ithaca, NY 14850	1

	Copies
Dr. D. Eccleshall U.S. Army Ballistic Research Lab. Aberdeen Proving Ground, MD 21005	1
Dr. Barbara Epstein Sandia Laboratories Albuquerque, NM 87185	1
Dr. A. Fisher Physics Dept. University of California Irvine, CA 92664	1
Dr. R. J. Faehl Los Alamos Scientific Lab. Los Alamos, NM 87544	1
Dr. Leon Feinstein Science Applications, Inc. 5 Palo Alto Square Palo Alto, CA 94304	1
Dr. Franklin Felber Western Research Corporation 8616 Commerce Ave. San Diego, CA 92121	1
Dr. Richard Fernslor Code 4770 Naval Research Lab. 4555 Overlook Ave., S.W. Washington, D.C. 20375	1
Dr. Thomas Fessenden Lawrence Livermore National Lab. L-321 University of California Livermore, CA 94550	1

DISTRIBUTION (Cont.)

	Copies
Dr. Robert Fossum, Director DARPA 1400 Wilson Boulevard Arlington, VA 22209	1
Dr. H. Freund Naval Research Lab. Code 4790 4555 Overlook Ave., S.W. Washington, D.C. 20375	1
Dr. M. Friedman Code 4700.1 Naval Research Laboratory Washington, D.C. 20375	1
Dr. B. Godfrey Mission Res. Corp. 1400 San Mateo Blvd, S.E. Suite A Albuquerque, NM 87108	1
Dr. T. Godlove Office of Inertial Fusion U.S. Department of Energy Washington, D.C. 20545	1
Dr. Jeffry Golden Naval Research Laboratory Washington, D.C. 20375	1
Dr. S. Goldstein Jaycor (Code 4770) Naval Research Lab. Washington, D.C. 20375	1
Dr. Victor Granatstein Naval Research Lab. Washington, D.C. 20375	1
Dr. S. Graybill Harry Diamond Lab. 2800 Powder Mill Rd. Adelphi, MD 20783	1
Dr. Michael Greenspan McDonnell Douglas Corp. St. Louis, MO 63166	1

	Copies
Dr. Robert Greig Naval Research Lab. (Code 4763) 4555 Overlook Ave., S.W. Washington, D.C. 20375	1
Dr. J.U. Guillory Jaycor 20050 Whiting St. Suite 500 Alexandria, VA 22304	1
Dr. Irving Haber Code 4790 Naval Research Lab. Washington, D.C. 20375	1
Prof. D. Hammer Lab. of Plasma Studies Cornell University Ithaca, NY 14850	1
Dr. Robert Hill Physics Division, #341 National Science Foundation Washington, D.C. 20550	1
Dr. J. L. Hirshfield Yale University Mason Laboratory 400 Temple Street New Haven, CT 06520	1
Dr. Richard Hubbard Code 4790 (Jaycor) Naval Research Lab. 4555 Overlook Ave., S.W. Washington, D.C. 20375	1
Dr. Bertram Hui Naval Research Lab. Code 4790 4555 Overlook Ave., S.W. Washington, D.C. 20375	1
Dr. S. Humphries Sandia Laboratories Albuquerque, NM 87115	1

DISTRIBUTION (Cont.)

	Copies
Dr. Robert Johnston Science Applications, Inc. 5 Palo Alto Square Palo Alto, CA 94304	1
Dr. Howard Jory Varian Associates, Bldg. 1 611 Hansen Way Palo Alto, CA 94303	1
Dr. Glenn Joyce Code 4790 Naval Research Lab. 4555 Overlock Ave., S.W Washington, D.C. 20375	1
Dr. Selig Kainer Naval Research Lab. 4555 Overlook Ave., S.W. Washington, D.C. 20375	1
Dr. C.A. Kapetanakos Plasma Physics Division Naval Research Laboratory Washington, D.C. 20375	1
Dr. Denis Keefe Lawrence Beskeley Lab. 1 Cyclotron Road Berkeley, CA 94720	1
Dr. Douglas Keeley Science Applications, Inc. 5 Palo Alto Square Palo Alto, CA 94304	1
Dr. Hogil Kim A & FR Div. Lawrence Berkeley Lab. Berkeley, CA 94720	1
Dr. Hong Chul Kim A & FR Div. Lawrence Berkeley Lab. Berkeley, CA 94720	1

	Copies
Dr. Kwang Je Kim Bldg. 64 #223 A & FR Div. Lawrence Berkeley Lab. Berkeley, CA 94720	1
Dr. Jin Joong Kim North Carolina State University Raleigh, NC 27607	1
Prof. N. M. Kroll La Jolla Institutes P.O. Box 1434 La Jolla, CA 92038	1
Dr. M. Lampe Naval Research Lab. Code 4790 4555 Overlook Ave., S.W. Washington, D.C. 20375	1
Dr. L. J. Laslett Lawrence Berkeley Lab. 1 Cyclotron Road Berkeley, CA 96720	1
Dr. Y. Y. Lau Naval Research Lab. Code 4740 (SAI) 4555 Overlook Ave., S.W. Washington, D.C. 20375	1
Dr. Glen R. Lambertson Lawrence Berkeley Lab. 1 Cyclotron Road, Bldg. 47 Berkeley, CA 94720	1
Dr. J. Carl Leader McDonnell Douglas Corp. Box 516 St. Louis, MO 63166	1

DISTRIBUTION (Cont.)

	Copies
Dr. W. M. Manheimer Naval Research Lab. Code 4790 4555 Overlook Ave., S. W. Washington, D. C. 20375	1
Dr. Edward P. Lee Lawrence Livermore National Lab L-321 University of California Livermore, CA 94550	1
Dr. Ray Lemke Air Force Weapons Lab Kirtland Air Force Base Albuquerque, NM 87117	1
Dr. Anthony T. Lin University of California Los Angeles, CA 90024	1
Dr. C. S. Liu Dept. of Physics University of Maryland College Park, MD 20742	1
Dr. Tom Lockner Sandia Laboratories Albuquerque, NM 87115	1
Dr. Conrad Longmire Mission Research Corp. 735 State Street Santa Barbara, CA 93102	1
Prof. R. V. Lovelace School of Applied and Eng. Physics Cornell University Ithaca, NY 14853	1
Dr. Joseph A. Mangano DARPA 1400 Wilson Blvd. Arlington, VA 22209	1

	Copies
Dr. James Mark L-477 Lawrence Livermore Lab Livermore, CA 94550	1
Dr. Jon A. Masamitsu Lawrence Livermore National Lab L-321 University of California Livermore, CA 94550	1
Dr. Bruce R. Miller Div. 5246 Sandia Laboratories Albuquerque, NM 87115	1
Dr. Melvin Month Department of Energy High Energy Physics Washington, D.C. 20545	1
Dr. Philip Morton Stanford Linear Accelerator Center P.O. Box 4349 Stanford, CA 94305	1
Dr. Don Murphy Naval Research Lab 4555 Overlook Ave., S.W. Washington, D.C. 20375	1
Dr. Won Namkung E. E. Department University of Maryland College Park, MD 20742	1
Prof. J. Nation Lab of Plasma Studies Cornell University Ithaca, NY 14850	1
Dr. V. Kelvin Neil Lawrence Livermore Nat'l Lab P.O. Box 808, L-321 Livermore, CA 94550	1

DISTRIBUTION (Cont.)

	Copies
Dr. Barry Newberger Mail Stop 608 Los Alamos National Lab Los Alamos, NM 87544	1
Dr. C. L. Olson Sandia Lab Albuquerque, NM 87115	1
Dr. Edward Ott Dept. of Physics University of Maryland College Park, MD 20742	1
Dr. Peter Palmadesso Bldg A50 #107 Naval Research Lab Washington, D.C. 20375	1
Dr. Ron Parkinson Science Applications, Inc. 1200 Prospect St. P.O. Box 2351 La Jolla, CA 92038	1
Dr. Richard Patrick AVCO - Everett Research Lab, Inc. 2385 Revere Beach Pkwy Everett, MA 02149	1
Dr. Robert Pechacek Naval Research Lab Code 4763 4555 Overlook Ave., S.W. Washington, D.C. 20375	1
Dr. Sam Penner National Bureau of Standards Bldg. 245 Washington, D.C. 20234	1
Dr. Michael Picone Naval Research Lab 4555 Overlook Ave., S.W. Washington, D.C. 20375	1
Dr. R. Post Lawrence Livermore Lab University of California P.O. Box 808 Livermore, CA 94550	1
Dr. D. S. Prono Lawrence Livermore Lab P.O. Box 808 Livermore, CA 94550	1
Dr. S. Putnam Physics Internal Co. 2700 Merced St. San Leandro, CA 94577	1
Dr. Sid Putnam Pulse Sciences, Inc. 1615 Broadway, Suite 610 Oakland, CA 94612	1
Dr. Michael Raleigh Naval Research Lab Code 4763 4555 Overlook Ave., S.W. Washington, D.C. 20375	1
Dr. M. E. Read Naval Research Lab Code 4740 4555 Overlook Ave., S.W. Washington, D.C. 20375	1
Prof. M. Reiser Dept. of Physics & Astronomy University of Maryland College Park, MD 20742	1
Dr. M. E. Rensink Lawrence Livermore Lab P.O. Box 808 Livermore, CA 94550	1
Dr. Moon-Jhong Rhee E. E. Department University of Maryland College Park, MD 20742	1

DISTRIBUTION (Cont.)

	Copies
Dr. C. W. Roberson Naval Research Lab Code 4740 4555 Overlook Ave., S.W. Washington, D.C. 20375	1
Dr. J. A. Rome Oak Ridge National Lab Oak Ridge, TN 37850	1
Dr. Marshall N. Rosenbluth University of Texas at Austin Inst. for Fusion Studies RLM 11.218 Austin, TX 78712	1
Prof. Norman Rostoker Dept. of Physics University of California Irvine, CA 92664	1
Dr. C. F. Sharn Naval Sea Systems Command Department of the Navy Washington, D. C. 20363	1
Prof. S. P. Schlesinger Columbia University Dept. of Electrical Engineering New York, NY 10027	1
Prof. George Schmidt Physics Dept. Stevens Institute of Technology Hoboken, NJ 07030	1
Dr. Andrew M. Sessler Lawrence Berkeley Lab Berkeley, CA 94720	1
Dr. J. D. Sethian Naval Research Lab Code 4762 Washington, D.C. 20375	1

	Copies
Dr. William Sharp Naval Research Lab Code 4790 (SAI) 4555 Overlook Ave., S.W. Washington, D.C. 20375	1
Dr. D. Straw AFWL Kirtland AFB, NM 87117	1
Dr. John Siambis Science Applications, Inc. 5 Palo Alto Square Palo Alto, CA 94304	1
Dr. J. S. Silverstein Code 4740 (HDL) Naval Research Lab 4555 Overlook Ave., S.W. Washington, D.C. 20375	1
Dr. M. Lee Sloan Austin Research Associates, Inc. 1901 Rutland Drive Austin, Texas 78758	1
Dr. L. Smith Lawrence Berkeley Lab 1 Cyclotron Road Berkeley, CA 94770	1
Dr. Joel A. Snow Senior Technical Advisor Office of Energy Research U.S. Department of Energy, M.S. E084 Washington, D.C. 20585	1
Dr. Philip Sprangle Naval Research Lab Code 4790 4555 Overlook Ave., S.W. Washington, D.C. 20375	1

DISTRIBUTION (Cont.)

	Copies
Dr. Doug Strickland Naval Research Lab Code 4790 (Beers) 4555 Overlook Ave., S W. Washington, D.C. 20375	1
Dr. Charles D. Striffler E. E. Dept. Univ. of Maryland College Park, MD 20742	1
Prof. R. Sudan Lab of Plasma Studies Cornell University Ithaca, NY 14850	1
Dr. C. M. Tang Naval Research Lab Code 4790 4555 Overlook Ave., S.W. Washington, D.C. 20375	1
Dr. R. Temkin Plasma Fusion Center Massachusetts Institute of Technology Cambridge, MA 02139	1
Dr. Lester E. Thode Mail Stop 608 Los Alamos National Lab Los Alamos, NM 87544	1
Dr. James R. Thompson Austin Research Associate, Inc. 1901 Rutland Drive Austin, Texas 78758	1
Dr. D. Tidman Jaycor 205 S. Whiting St. Alexandria, VA 22304	1
Dr. A. W. Trivelpiece Science Applications, Inc. San Diego, CA 92123	1

	Copies
Dr. John E. Walsh Department of Physics Dartmouth College Hanover, NH 03755	1
Dr. Wasneski Naval Air Systems Command Department of the Navy Washington, D.C. 20350	1
Dr. N. R. Vanderplaats Naval Research Laboratory Code 6805 4555 Overlook Ave., S. W. Washington, D.C. 20375	1
Lt. Col. W. Whitaker Defense Advanced Research Projects Agency 1400 Wilson Boulevard Arlington, VA 22209	1
Dr. Mark Wilson National Bureau of Standards Gaithersburg, MD 20760	1
Dr. Gerold Yonas Sandia Lab Albuquerque, NM 87115	1
Dr. Simon S. Yu Lawrence Livermore National Lab L-321 University of California Livermore, CA 94550	1
Defense Technical Information Center Cameron Station Alexandria, VA 22314	12

Internal distribution:

R	1
R04	1
R40	1

DISTRIBUTION (Cont.)

Internal Distribution (Cont.)	Copies
R401	1
R43 (C. W. Lufcy)	1
R44 (T. F. Zien)	1
R45 (H. R. Riedl)	1
R13 (J. Forbes)	1
R41 (P. O. Hesse)	1
R41 (R. Cawley)	1
R41 (M. H. Cha)	1
R41 (H. C. Chen)	1
R41 (J. Y. Choe)	1
R41 (R. Fiorito)	1
R41 (O. F. Goktepe)	1
R41 (M. J. Rhee)	1
R41 (D. W. Rule)	1
R41 (Y. C. Song)	1
R41 (H. S. Uhm)	1
R43 (A. D. Krall)	1
F	1
F14 (H. C. Coward)	1
F40 (J. F. Cavanagh)	1
F10 (K. C. Baile)	1
F46 (D. G. Kirkpatrick)	1
F34 (R. A. Smith)	1
F34 (E. Nolting)	1
F34 (V. L. Kenyon)	1
F04 (M. F. Rose)	1
F34 (F. Sazama)	1
N14 (R. Biegalski)	1
E431	9
E432	3
E35	1

4-8

DTI